Ultrasonically induced microscopic refractive index gradient and the relationship with high-frequency ultrasonic cavitation

Y. Harada,[1] M. Ishikawa,[2] M. Matsukawa,[1] and D. Koyama[1,a]

AFFILIATIONS

[1]Faculty of Science and Engineering, Doshisha University, 1-3 Tataramiyakodani, Kyotanabe, Kyoto 610-0321, Japan
[2]Faculty of Biomedical Engineering, Toin University of Yokohama, 1641 Kurokane, Aoba, Yokohama, Kanagawa 225-8503, Japan

[a]Author to whom correspondence should be addressed: dkoyama@mail.doshisha.ac.jp

ABSTRACT

The refractive index of a medium can be modulated by external stimuli such as pressure, temperature, or electromagnetic forces. This principle enables fast, precise, and reversible optical control and has catalyzed the development of optical devices and optical measurement technology. Here, we report the relationship between the refractive index change induced by high-frequency ultrasonic irradiation and ultrasonic cavitation. The cavitation nanobubbles generated by ultrasonic irradiation were measured using dynamic light scattering to be approximately 100 nm in diameter. The apparent volume fraction of the nanobubbles induced near the surface of the ultrasonic transducer was calculated using an effective medium approximation. The apparent volume fraction was 0.12 at the position where the refractive index change was maximal ($\Delta n = 0.04$: value from the fitting function). The technique to control light propagation in a local (microscale) region with ultrasonic irradiation has a wide range of applications from optofluidic devices for lab-on-chip devices to variable-focus lenses for industrial metrology.

I. INTRODUCTION

The propagation of light can be controlled by dynamically moving optical components such as lenses and mirrors. Optical instruments based on this technique enable visualization of objects over a wide range of scales from the microscopic to the astronomical and are essential tools for scientific innovation. However, these techniques typically require mechanically moving parts to change the positions and angles of optical components, which is a bottleneck for miniaturization and rapid response of devices. For instance, cameras are now being integrated into small electronic devices such as smartphones, and there is a strong demand for thin, compact, robust devices that can deliver high performance. In recent years, metalenses, which are thinner than conventional lenses, have attracted attention for their potential use in ultracompact optical devices. Although traditional metalenses are fixed once fabricated, several designs now offer dynamic control.[1–3] However, tunable metalenses have limitations, such as slow response times, limited optical bandwidth, and high optical loss.[1,4]

The light propagation in a medium can be controlled in a fast, reversible, and flexible manner by modulating the refractive index of the medium by using external stimuli such as pressure (e.g., density changes), electromagnetic forces, and temperature. This spatially flexible technique can be implemented in devices ranging in size from variable-focus gradient-index (GRIN) lenses (millimeter scale) for use in industrial inspection, metrology, or laser processing[5–7] to optofluidic devices (nano- to microscale) for use in lab-on-a-chip technology.[8,9] Since the refractive index of a medium is a function of its density,[10,11] ultrasonic waves, a type of pressure variation, are one of the major methods of refractive index modulation. For example, acousto-optic (AO) devices such as tunable acoustic gradient (TAG) lenses[12,13] enable high-speed and high-precision optical control using ultrasonic waves and are used in a wide range of research and industrial fields. However, this refractive index modulation is enabled by dynamic changes (i.e., the refractive index changes with time) induced by ultrasonic standing waves and cannot statically refract light like conventional optical lenses, mirrors, or prisms. In addition,

the refractive index that ultrasonic waves can modulate in a single medium is very small ($\Delta n = 10^{-4}$–10^{-5}),[11,14] limiting the range of controllable light propagation.

We have devised techniques for controlling the refractive index using the radiation force of ultrasound waves (acoustic radiation force: static pressure)[15,16] and developed ultrasonic optical devices such as variable-focus lenses.[17–20] These optical devices utilize acoustic radiation forces to change the refractive index, allowing for the static control of light propagation. We found that a large refractive index gradient ($\Delta n = 10^{-2}$–10^{-3}) was induced by high intensity (on the order of 1 MPa) ultrasonic irradiation in the 100-megahertz range in water.[21] However, the mechanism of this phenomenon is still under investigation, and we currently consider ultrasonic cavitation to be the main process. Ultrasonic cavitation is a phenomenon in which bubbles are generated and violently collapse in a liquid under strong ultrasonic irradiation. Various studies of this effect have been conducted, particularly in the fields of sonoluminescence and sonochemistry.[22,23] In this paper, we analyzed the size distribution of nanobubbles generated by ultrasonic irradiation at 160 MHz using dynamic light scattering (DLS). Furthermore, the nanobubble density distribution induced near the surface of the ultrasonic transducer was calculated by obtaining the volume fraction from the refractive index gradient model using the effective medium approximation (EMA). The technology of controlling refractive index in a local (microscale) area using ultrasonic irradiation may have applications for optofluidic devices, such as MEMS variable-focus lenses[24] and optical waveguides.[25]

II. MATERIALS AND METHODS

A. Refractive index gradient induced by high-frequency high-intensity ultrasonic irradiation

In this study, a potassium niobate (KNbO$_3$) piezoelectric film was used to fabricate the ultrasonic transducer for irradiating high-frequency, high-intensity ultrasonic waves in a liquid (the supplementary material). The KNbO$_3$ piezoelectric film was deposited on a (100)c Nb-SrTiO$_3$ substrate using the hydrothermal method at 240 °C, and the film thickness was increased to approximately 70 μm through repeated reactions.[26,27] A continuous sinusoidal electric signal with a frequency of 160 MHz was generated by a function generator (T3AFG500, Teledyne Technologies) and amplified to 50 dB using a high-frequency amplifier (ZCA5050-9K250M-OR, RAD) to excite the KNbO$_3$ ultrasonic transducer. The surface of the KNbO$_3$ ultrasonic transducer was designed to be flat so that high-frequency, high-intensity plane wave ultrasound was irradiated into a

liquid. Figure 1 shows the refractive index change observed when high-frequency, high-intensity ultrasound waves (ultrasonic frequency: 160 MHz, input voltage: 92 V_{PP}) were irradiated into the water in a previous study.[21] In Fig. 1, a grid panel was placed behind the ultrasonic transducer, and the refractive index change induced by ultrasonic irradiation distorts the grid toward the ultrasonic transducer. This is because the refractive index of water changed in the direction of approaching that of air in the area where the refractive index changed due to ultrasonic irradiation. On the other hand, we have irradiated ultrasonic waves into a solid (quartz glass) using a KNbO$_3$ ultrasonic transducer; however, this phenomenon has so far only been observed in liquids. Furthermore, when high-frequency, high-intensity ultrasonic waves (ultrasonic frequency: 160 MHz, input voltage: 101 V_{PP}) were continuously irradiated, microbubbles were observed on the surface of the ultrasonic transducer (the supplementary material). Observations of this refractive index region were conducted using a long-distance microscope (QM100, Questar) and a high-speed camera (HPV-1, Shimadzu) with a spatial resolution of less than 1 μm/pixel.[28] However, the presence of microbubbles could not be confirmed, suggesting that the bubble size in the area of refractive index change was at 1 μm or smaller.

B. Evaluation of high-frequency ultrasonic cavitation

The DLS method and nanoparticle tracking analysis (NTA) are widely used for measuring nanobubble sizes.[29,30] Both techniques rely on the Brownian motion of fine particles. The DLS method calculates the particle size based on the intensity changes in scattered light caused by this motion, and NTA tracks the motion of individual particles. Although NTA has higher resolution, it is generally unsuitable for high-concentration samples and limited to a narrow size range (on the order of nanometers). By contrast, DLS can measure a wide range of particle sizes (0.6 nm–10 μm), handle relatively high concentrations, has a simple procedure, and offers a short measurement time.[31] In this study, we used the DLS method to evaluate the particle size distribution of nanobubbles generated in ultrapure water by ultrasonication. A glass cell was filled with ultrapure water (1.5 ml filled with a micropipet, pH: 7.1 as determined by a pH meter), and high-frequency, high-intensity ultrasonic waves (frequency: 160 MHz, input voltage: 101 V_{PP}) were irradiated continuously for 60 s. Ultrasonication was repeated for 50 cycles, and the particle size distribution of the nanobubbles generated in the glass cell was measured between each cycle with a DLS measurement system (ELSZ-2000, Otsuka Electronics, Osaka, Japan). All DLS measurements were conducted
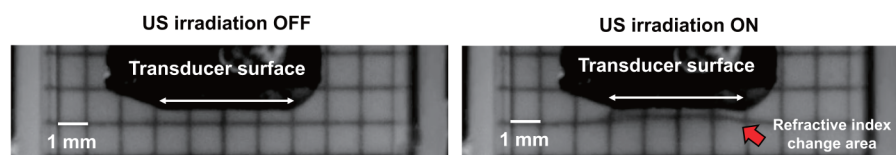

FIG. 1. Photograph of the spatial distribution of the refractive index change (Δn) caused by high-frequency, high-intensity ultrasonic wave radiation (ultrasonic frequency: 160 MHz, input voltage: 92 V_{PP}). The image was taken using a high-speed camera and a grid panel. Reproduced with permission from Harada *et al.*, Appl. Phys. Lett. **124**, 011102 (2024). Copyright 2024 AIP Publishing LLC.

under stable conditions with a sample temperature of 25 °C. To guarantee the measurement accuracy of the DLS method, it is necessary that the nanobubble concentration in the sample exceeds a specific threshold. Consequently, measurements were conducted after slightly longer ultrasonication times (a few seconds) than those required to obtain a steady-state refractive index gradient. Although each DLS measurement took several minutes, it has been confirmed that nanobubbles generally have a long lifetime,[30] so it was possible to confirm the presence of nanobubbles in the sample with this measurement time. In addition, we evaluated the zeta potential, the change in dissolved oxygen (DO) content, and the change in pH of the samples after ultrasonication (the supplementary material). The zeta potential is an important parameter that controls electrostatic interactions in colloidal dispersions and is used as an indication of the stability of nanobubbles in a measurement sample. The zeta potential and pH change of the sample were measured after 50 cycles of ultrasonication. The DO change in the sample was measured three times after each ultrasonication cycle (50 cycles at 160 MHz, 101 V_{PP}).

C. Nanobubble density distribution near the surface of the ultrasonic transducer calculated using effective medium approximation (EMA)

We considered the relationship between the refractive index change and the nanobubbles induced by ultrasonic irradiation. In a previous study,[32] we found that the area of refractive index change [$n(x, y)$] induced near the surface of an ultrasonic transducer can be roughly modeled with a two-dimensional Gaussian distribution. Therefore, the apparent volume fraction of the nanobubbles (area of refractive index change) was calculated using an EMA.[33,34] An EMA is a general method for calculating the effective dielectric function of a layer, assuming that a layer of spherical particles

(nanobubbles in this study) is dispersed with a certain volume fraction in a matrix material (water in this study). The apparent volume fraction of the nanobubbles was calculated from the refractive index change (dielectric constant change) at each position using the Bruggeman model (EMA model) shown in Eq. (1),

$$(1 - f_b)\frac{\varepsilon_m - \varepsilon_{eff}}{\varepsilon_m + 2\varepsilon_{eff}} + f_b\frac{\varepsilon_p - \varepsilon_{eff}}{\varepsilon_p + 2\varepsilon_{eff}} = 0. \qquad (1)$$

In Eq. (1), f_b represents the apparent volume ratio of the particles to the matrix (volume fraction of nanobubbles), ε_m is the dielectric constant of the matrix material (i.e., water; $\varepsilon_m = 1.77$), ε_{eff} is the dielectric constant in the area in which the refractive index changes [i.e., the dielectric constant of water minus the dielectric constant change $\Delta\varepsilon = (\Delta n)^2$], and ε_p is the dielectric constant of the particles (i.e., the dielectric constant of nanobubbles; $\varepsilon_p = 1.00$). In other words, the distribution of the refractive index change was converted to a dielectric function distribution, which was then converted to a function of volume fraction to calculate the local volume fraction based on the refractive index change.

III. RESULTS AND DISCUSSION

Figure 2 shows the particle size distribution of nanobubbles in the sample after 15 cycles of ultrasonication, as measured by using the DLS method; notably, three peaks are present. The first peak was observed at around 10 nm (peak 1 in Fig. 2) and was occasionally observed before ultrasonication. Therefore, we do not consider peak 1 to be the result of nanobubbles generated by ultrasonication and excluded it from our analysis. Peaks at several hundred nm (peak 2) and several hundred micrometers (peak 3) were also observed. Peak 3 changed significantly with each measurement,
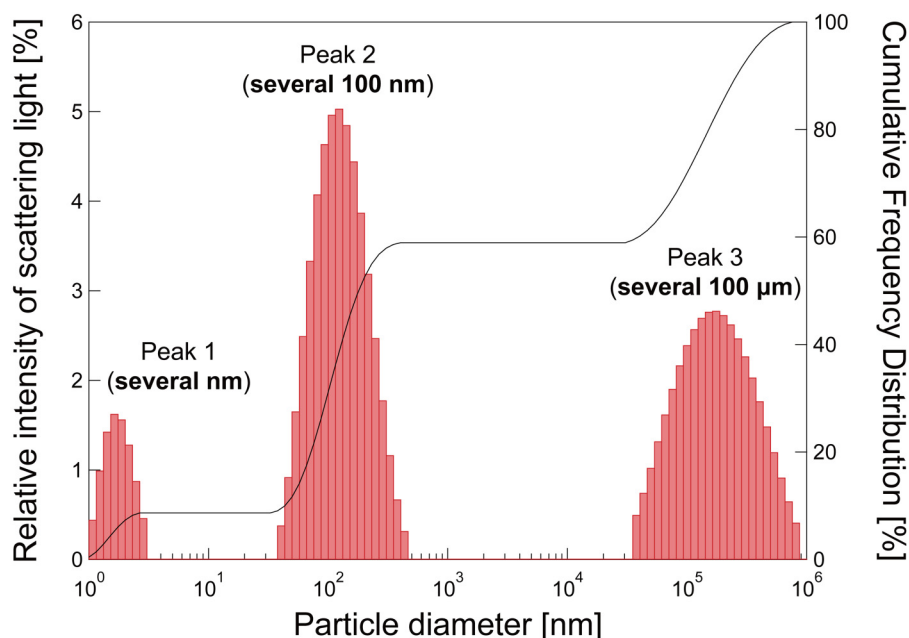

FIG. 2. Observed peaks of the particle size distribution after 15 cycles of ultrasonication (frequency: 160 MHz voltage: 101 V_{PP}) measured by dynamic light scattering (DLS).

indicating a high possibility of microbubbles generated by ultrasonic irradiation or contamination during the experiment.

Transmission electron microscope (TEM) measurements were also conducted to evaluate the presence of solid particles in the sample after ultrasonication (the supplementary material). When erosion caused by ultrasonic cavitation occurred on the surface of the ultrasonic transducer, the gold electrode formed by vacuum deposition peeled off and was mixed into the measurement sample. However, TEM measurement results did not show any solid particles such as gold particles in the measurement sample. Therefore, we surmised that peak 2 represents nanobubbles generated by ultrasonication, and we evaluated the change in the average size of nanobubbles. Figure 3 shows the average particle size of nanobubbles, and its standard deviation observed after each ultrasonication cycle. The average particle size of the nanobubbles was on the order of 100 nm for ultrasonication cycles 7–20.

Bubble generation by ultrasonic irradiation in the megahertz range has been frequently reported in the literature, and it is known that the cavitation threshold of sound pressure depends on the ultrasonic frequency.[35–37] Although the ultrasonic frequency in their study was much lower than in this study, Yasuda et al. reported that the diameter of nanobubbles generated during ultrasonication of ultrapure water with a frequency of 22 kHz–1 MHz was about 90–100 nm,[38] which corresponds to the diameter of the nanobubbles observed in Fig. 3. Moreover, we evaluated the time dependence of the measurement after 15 cycles of ultrasonication (160 MHz, 101 V_{pp}, 60 s). However, no significant change in particle diameter was observed after tens of minutes (the supplementary material). After 2 days, there was still no significant change in nanobubble size. Furthermore, the average diameter of nanobubbles and its standard deviation exhibited a tendency to increase with the
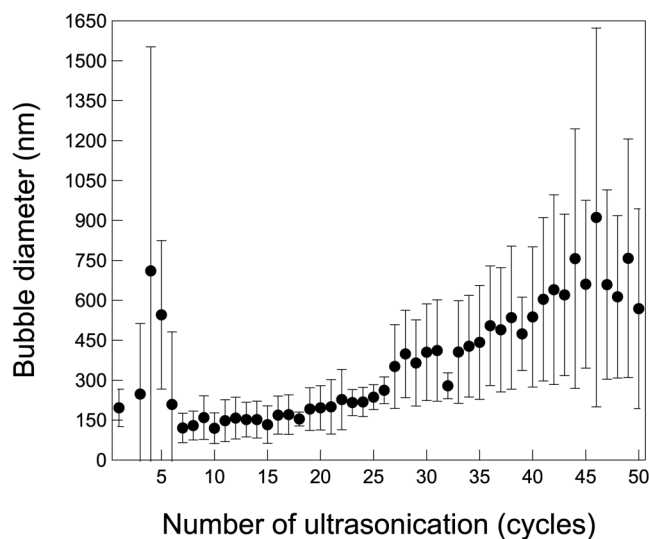
ultrasonication cycles as shown in Fig. 3. This suggests that larger nanobubbles may be generated as the cycles of ultrasonication increases. A similar tendency was observed for D50 (median diameter), with the particle size in the measured sample increasing as the number of ultrasonic irradiations increased (the supplementary material). This may be because DLS is more sensitive to large particles than to small particles, and the concentration of large particles may have been relatively high. However, we believe that the main cause of this trend was the agglomeration or coalescence of nanobubbles due to secondary Bjerknes forces.[28,39–41] As the concentration of nanobubbles in the measurement sample increased with the ultrasonication cycles, the distances between the nanobubbles decreased. Although the ultrasonic radiation forces acting on individual nanobubbles are weak (the volume of nanobubbles is small), secondary Bjerknes forces are inversely proportional to the square of the distances between nanobubbles, which is thought to cause smaller bubbles to agglomerate or coalesce into large bubbles. It should be noted that DLS only measures the change in the average particle size of nanobubbles in a sample (not the change in the average particle size of nanobubbles for a constant number of nanobubbles). Consequently, it is not possible to quantitatively assess the agglomeration and coalescence of nanobubbles due to the secondary Bjerknes force. We will investigate nanobubble agglomeration and coalescence using the NTA method in future work. Next, the zeta potential ranged from −10 to −30 mV (average of −25.2 mV) and the average pH was 6.2 at a temperature of 25 °C (Fig. 4). Nanobubbles are well known to be negatively charged on the order of −10 to −50 mV,[42–45] so the negative zeta potential measured in the present sample indicates the possibility of the generation of stable nanobubbles. The pH changed in the direction of oxidation owing to ultrasonication but remained close to neutral. In addition, our measurements showed that the DO content tended to decrease as the ultrasonication cycle increased (the supplementary material). This was because of the release of large bubbles formed from the agglomeration and coalescence of nanobubbles or microbubbles into the atmosphere.
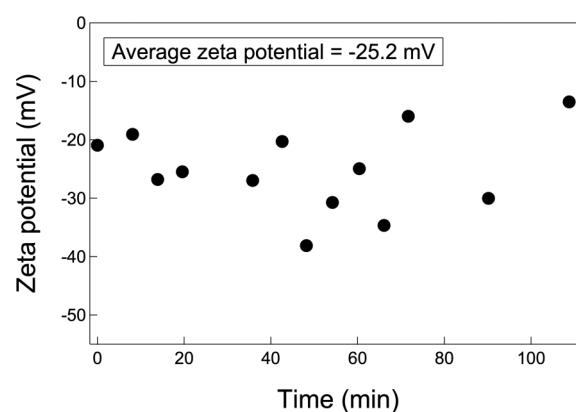

FIG. 3. Relationship between the number of ultrasonication cycles (50 cycles, ultrasonic frequency: 160 MHz, input voltage: 101 V_{pp}) and the average diameter of nanobubbles in the sample.

FIG. 4. Temporal variation in the zeta potential of fine particles in the sample after ultrasonication for 50 cycles (ultrasonic frequency: 160 MHz, input voltage: 101 V_{pp}).

Finally, nanobubble density distribution near the surface of the ultrasonic transducer was calculated by obtaining the apparent volume fraction from the refractive index gradient model using an EMA. It should be noted that EMAs are applicable to phases or dielectrics of a sufficiently small order of magnitude ($\lambda/10$) relative to the radiation wavelength (λ). In this study, nanobubbles in the size range of about 100 nm or less (the resonance radius of bubbles calculated from the Minnaert equation is approximately 18 nm for 160 MHz ultrasonic irradiation) were investigated. The apparent volume fraction of nanobubbles with diameters on the order of 10–100 nm can be calculated and is considered to be within the applicable range.[46,47] Equation (2) is the empirical formula based on the experimental results of our previous study;[32] this formula was obtained by fitting the function converted form of the refractive index gradient model [$= n(x, y)$] to a volume fraction model [$= f(x, y)$] using Eq. (1). In other words, it is possible to express changes in physical values (refractive index, dielectric constant, and volume fraction) at each position in a two-dimensional coordinate space (x-coordinate, y-coordinate) through each mathematical

model. Therefore, the volume fraction of the local region was calculated based on the refractive index change by first converting the refractive index gradient model to a dielectric constant model, and then further converting it to a volume fraction model using the Bruggeman model [Eq. (1)],

$$f_b(x, y) = 0.12 \exp\left(-(3.5x^2) - \left(\frac{y - 0.34}{-0.3}\right)^2\right). \quad (2)$$

Figure 5 shows the nanobubble density distribution induced near the surface of the ultrasonic transducer. Figure 5(a) shows the profile of the apparent volume fraction of the nanobubbles calculated using Eq. (2). Figures 5(b) and 5(c) show that the maximum value of f_b was 0.12 and that the width of change in the apparent volume fraction distribution in the radial direction at $y = 0.34$ ($= |x|$) was approximately 2.0 mm.

The apparent volume fraction distribution in Fig. 5(a) corresponds to the area where the refractive index change occurs during
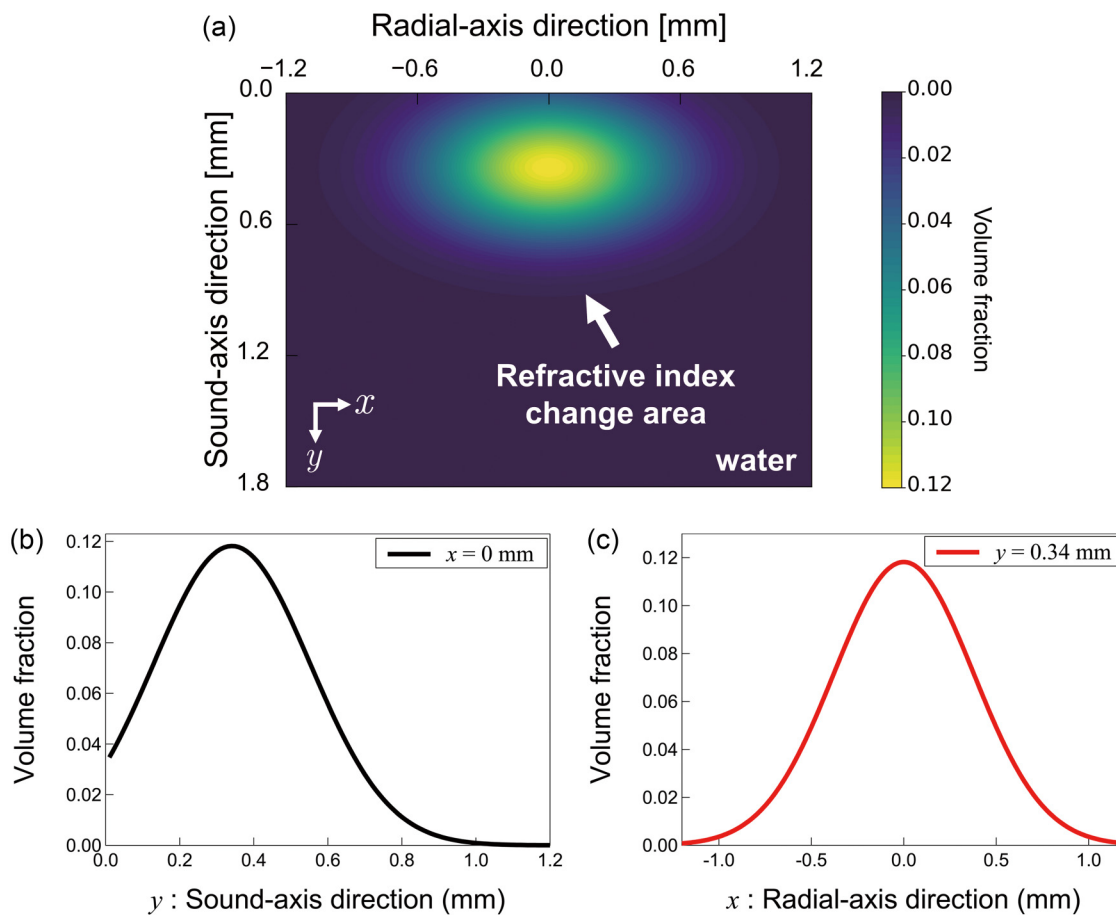
FIG. 5. Nanobubble density distribution (area of refractive index change) induced near the surface of the ultrasonic transducer. (a) Profile of the apparent volume fraction of the nanobubbles calculated by using an effective medium approximation (EMA). (b) Change in the apparent volume fraction in the direction of sound propagation at $x = 0$ mm. (c) Change in the apparent volume fraction along the radial axis at $y = 0.34$ mm.

ultrasonic irradiation in Fig. 1. However, it should be noted that the refractive index change (approximately 3.5 mm in the radial axial direction) observed in Fig. 1 was slightly larger in the radial direction than the nanobubble density distribution (approximately 2.0 mm in the radial axial direction) in Fig. 5(a). In this study, the apparent volume fraction was calculated using a two-dimensional Gaussian distribution for simplicity. Therefore, a function for which the apparent volume fraction decreases more gradually in the radial-axis direction at the position where the change in apparent volume fraction was maximal [$y = 0.3$–0.4 mm in Fig. 5(a)] may be more preferable based on the results in Fig. 1. We will consider different fitting functions in a future study. It should be noted that the volume fraction model was derived from the refractive index model established in previous research, without addressing the mechanism of nanobubble cluster generation. Future research should focus on a detailed investigation of the relationship between the ultrasonic field and the refractive index distribution. The takeaway is that, as shown in Fig. 1, the refractive index change was not influenced by light scattering in the region where the refractive index change occurred, and distortion of the grid lines was clearly visible. This suggests that the ultrafine bubbles clustered without being affected by light scattering.[48] We hypothesize that the processes of nanobubble formation, growth, agglomeration, coalescence, and collapse may be repeated in the area of refractive index change. Furthermore, it is noteworthy that the induced refractive index change can be controlled only by adjusting the parameters of ultrasonic irradiation.

IV. CONCLUSION

We investigated the relationship between refractive index change and ultrasonic cavitation generated by high-intensity ultrasonic irradiation at 160 MHz. First, the particle sizes of the nanobubbles present in the sample after ultrasonication were evaluated using DLS, and results showed that nanobubbles with diameters of approximately 100 nm were generated. Furthermore, the average particle size of the observed nanobubbles tended to increase as the number of ultrasonication cycles increased, which was attributed to secondary Bjerknes forces. Finally, the nanobubble density distribution induced near the transducer surface during ultrasonic irradiation was calculated using an effective medium approximation (EMA). The calculated result showed that the maximal volume fraction was 0.12 (refractive index change: $\Delta n = 0.04$). In future work, we will develop ultrasonic optical devices based on this demonstrated capability of controlling the refractive index of liquid materials using high-frequency, high-intensity ultrasound.

SUPPLEMENTARY MATERIAL

See the supplementary material for high-frequency, high-intensity ultrasonic transducer, sample preparation for high-frequency cavitation evaluation, evaluation method, and results of high-frequency cavitation (dynamic light scattering, electrophoretic light scattering, dissolved oxygen, pH change, TEM, and EDS).

ACKNOWLEDGMENTS

AUTHOR DECLARATIONS

Conflict of Interest

The authors have no conflicts to disclose.

Author Contributions

Y. Harada: Conceptualization (equal); Data curation (equal); Formal analysis (equal); Funding acquisition (equal); Investigation (equal); Methodology (equal); Project administration (equal); Resources (equal); Software (equal); Validation (equal); Visualization (equal); Writing – original draft (equal); Writing – review & editing (equal). **M. Ishikawa:** Project administration (equal); Resources (equal); Supervision (equal). **M. Matsukawa:** Resources (equal); Supervision (equal). **D. Koyama:** Conceptualization (equal); Data curation (equal); Formal analysis (equal); Funding acquisition (lead); Methodology (equal); Project administration (equal); Resources (lead); Supervision (lead); Validation (lead); Writing – original draft (equal); Writing – review & editing (lead).

DATA AVAILABILITY

The data that support the findings of this study are available from the corresponding author upon reasonable request.

REFERENCES

[1] H.-S. Ee and R. Agarwal, "Tunable metasurface and flat optical zoom lens on a stretchable substrate," Nano Lett. **16**(4), 2818–2823 (2016).
[2] M. Y. Shalaginov, S. An, Y. Zhang, F. Yang, P. Su, V. Liberman, J. B. Chou, C. M. Roberts, M. Kang, C. Rios, Q. Du, C. Fowler, A. Agarwal, K. A. Richardson, C. Rivero-Baleine, H. Zhang, J. Hu, and T. Gu, "Reconfigurable all-dielectric metalens with diffraction-limited performance," Nat. Commun. **12**(1), 1225 (2021).
[3] A. Afridi, J. Gieseler, N. Meyer, and R. Quidant, "Ultrathin tunable optomechanical metalens," Nano Lett. **23**(7), 2496–2501 (2023).
[4] M. D. Aiello, A. S. Backer, A. J. Sapon, J. Smits, J. D. Perreault, P. Llull, and V. M. Acosta, "Achromatic varifocal metalens for the visible spectrum," ACS Photonics **6**(10), 2432–2440 (2019).
[5] M. Duocastella and C. B. Arnold, "Enhanced depth of field laser processing using an ultra-high-speed axial scanner," Appl. Phys. Lett. **102**(6), 061113 (2013).
[6] C. Huang, Y. Sasaki, J. Miyazu, S. Toyoda, T. Imai, and J. Kobayashi, "Trapped charge density analysis of KTN crystal by beam path measurement," Opt. Express **22**(7), 7783 (2014).
[7] S. Kang, E. Dotsenko, D. Amrhein, C. Theriault, and C. B. Arnold, "Ultra-high-speed variable focus optics for novel applications in advanced imaging," Proc. SPIE **10539**, 1053902 (2018).
[8] Q. Chen, A. Jian, Z. Li, and X. Zhang, "Optofluidic tunable lenses using laser-induced thermal gradient," Lab Chip **16**(1), 104–111 (2016).
[9] H. L. Liu, Y. Shi, L. Liang, L. Li, S. S. Guo, L. Yin, and Y. Yang, "A liquid thermal gradient refractive index lens and using it to trap single living cell in flowing environments," Lab Chip **17**(7), 1280–1286 (2017).
[10] M. Duocastella and C. B. Arnold, "Transient response in ultra-high speed liquid lenses," J. Phys. D: Appl. Phys. **46**(7), 075102 (2013).

22 March 2025 09:28:20

[11]M. Chamanzar, M. G. Scopelliti, J. Bloch, N. Do, M. Huh, D. Seo, J. Iafrati, V. S. Sohal, M.-R. Alam, and M. M. Maharbiz, "Ultrasonic sculpting of virtual optical waveguides in tissue," Nat. Commun. **10**(1), 92 (2019).

[12]A. Mermillod-Blondin, E. McLeod, and C. B. Arnold, "High-speed varifocal imaging with a tunable acoustic gradient index of refraction lens," Opt. Lett. **33**(18), 2146 (2008).

[13]X. Du, C. Florian, and C. B. Arnold, "Multi-focal laser processing in transparent materials using an ultrafast tunable acoustic lens," Opt. Lett. **47**(7), 1634 (2022).

[14]M. Duocastella, S. Surdo, A. Zunino, A. Diaspro, and P. Saggau, "Acousto-optic systems for advanced microscopy," J. Phys.: Photonics **3**(1), 012004 (2021).

[15]S. Taniguchi, D. Koyama, Y. Shimizu, A. Emoto, K. Nakamura, and M. Matsukawa, "Control of liquid crystal molecular orientation using ultrasound vibration," Appl. Phys. Lett. **108**(10), 101103 (2016).

[16]Y. Shimizu, D. Koyama, S. Taniguchi, A. Emoto, K. Nakamura, and M. Matsukawa, "Periodic pattern of liquid crystal molecular orientation induced by ultrasound vibrations," Appl. Phys. Lett. **111**(23), 231101 (2017).

[17]Y. Shimizu, D. Koyama, M. Fukui, A. Emoto, K. Nakamura, and M. Matsukawa, "Ultrasound liquid crystal lens," Appl. Phys. Lett. **112**(16), 161104 (2018).

[18]Y. Harada, D. Koyama, M. Fukui, A. Emoto, K. Nakamura, and M. Matsukawa, "Molecular orientation in a variable-focus liquid crystal lens induced by ultrasound vibration," Sci. Rep. **10**(1), 6168 (2020).

[19]S. Hashimoto, Y. Harada, K. Nakamura, T. Iwase, J. Onaka, M. Matsukawa, and D. Koyama, "Varifocal concave–convex lens using viscoelastic gel and ultrasound vibration," IEEE Trans. Ultrason., Ferroelectr., Freq. Control **69**(9), 2703–2710 (2022).

[20]K. Tagashira, Y. Harada, K. Nakamura, H. Miki, M. Matsukawa, and D. Koyama, "Focus control of a concave–convex ultrasonic gel lens in the radial direction," J. Appl. Phys. **136**(11), 113101 (2024).

[21]Y. Harada, M. Ishikawa, Y. Kuroda, M. Matsukawa, and D. Koyama, "Giant static refractive index gradient induced by strong ultrasonic wave," Appl. Phys. Lett. **124**(1), 011102 (2024).

[22]K. S. Suslick, "The chemical effects of ultrasound," Sci. Am. **260**(2), 80–86 (1989).

[23]T. G. Leighton, *The Acoustic Bubble* (Academic Press, 1994).

[24]S. Nagelberg, L. D. Zarzar, N. Nicolas, K. Subramanian, J. A. Kalow, V. Sresht, D. Blankschtein, G. Barbastathis, M. Kreysing, T. M. Swager, and M. Kolle, "Reconfigurable and responsive droplet-based compound micro-lenses," Nat. Commun. **8**(1), 14673 (2017).

[25]H. L. Liu, X. Q. Zhu, L. Liang, X. M. Zhang, and Y. Yang, "Tunable transformation optical waveguide bends in liquid," Optica **4**(8), 839 (2017).

[26]M. Ishikawa, H. Einishi, M. Nakajima, T. Hasegawa, T. Morita, Y. Saijo, M. Kurosawa, and H. Funakubo, "Effect of deposition time on film thickness and their properties for hydrothermally-grown epitaxial KNbO₃ thick films," Jpn. J. Appl. Phys. **49**(7S), 07HF01 (2010).

[27]A. Tateyama, Y. Ito, Y. Nakamura, T. Shimizu, Y. Orino, M. Kurosawa, H. Uchida, T. Shiraishi, T. Kiguchi, T. J. Konno, T. Yoshimura, and H. Funakubo, "Good piezoelectricity of self-polarized thick epitaxial (K,Na)NbO₃ films grown below the Curie temperature (240 °C) using a hydrothermal method," Appl. Phys. Lett. **117**(14), 142903 (2020).

[28]K. Yoshida, T. Fujikawa, and Y. Watanabe, "Experimental investigation on reversal of secondary Bjerknes force between two bubbles in ultrasonic standing wave," J. Acoust. Soc. Am. **130**(1), 135–144 (2011).

[29]B. J. Berne and R. Pecora, *Dynamic Light Scattering: With Applications to Chemistry, Biology, and Physics* (Courier Corporation, 2000).

[30]N. Nirmalkar, A. W. Pacek, and M. Barigou, "On the existence and stability of bulk nanobubbles," Langmuir **34**(37), 10964–10973 (2018).

[31]A. Bootz, V. Vogel, D. Schubert, and J. Kreuter, "Comparison of scanning electron microscopy, dynamic light scattering and analytical ultracentrifugation for the sizing of poly(butyl cyanoacrylate) nanoparticles," Eur. J. Pharm. Biopharm. **57**(2), 369–375 (2004).

[32]Y. Harada, M. Ishikawa, Y. Kuroda, M. Matsukawa, and D. Koyama, "Simulation of light propagation in medium with an ultrasonically induced refractive index gradient," J. Appl. Phys. **135**(19), 193104 (2024).

[33]D. A. G. Bruggeman, "Berechnung verschiedener physikalischer Konstanten von heterogenen Substanzen. I. Dielektrizitätskonstanten und Leitfähigkeiten der Mischkörper aus isotropen Substanzen," Ann. Phys. **416**(7), 636–664 (1935).

[34]D. E. Aspnes, J. B. Theeten, and F. Hottier, "Investigation of effective-medium models of microscopic surface roughness by spectroscopic ellipsometry," Phys. Rev. B **20**(8), 3292–3302 (1979).

[35]R. E. Apfel and C. K. Holland, "Gauging the likelihood of cavitation from short-pulse, low-duty cycle diagnostic ultrasound," Ultrasound Med. Biol. **17**(2), 179–185 (1991).

[36]A. Brotchie, F. Grieser, and M. Ashokkumar, "Effect of power and frequency on bubble-size distributions in acoustic cavitation," Phys. Rev. Lett. **102**(8), 084302 (2009).

[37]T. Thanh Nguyen, Y. Asakura, S. Koda, and K. Yasuda, "Dependence of cavitation, chemical effect, and mechanical effect thresholds on ultrasonic frequency," Ultrason. Sonochem. **39**, 301–306 (2017).

[38]K. Yasuda, H. Matsushima, and Y. Asakura, "Generation and reduction of bulk nanobubbles by ultrasonic irradiation," Chem. Eng. Sci. **195**, 455–461 (2019).

[39]L. A. Crum, "Bjerknes forces on bubbles in a stationary sound field," J. Acoust. Soc. Am. **57**(6), 1363–1370 (1975).

[40]R. Mettin, I. Akhatov, U. Parlitz, C. Ohl, and W. Lauterborn, "Bjerknes forces between small cavitation bubbles in a strong acoustic field," Phys. Rev. E **56**(3), 2924–2931 (1997).

[41]K. Yasui, Y. Iida, T. Tuziuti, T. Kozuka, and A. Towata, "Strongly interacting bubbles under an ultrasonic horn," Phys. Rev. E **77**(1), 016609 (2008).

[42]N. Nirmalkar, A. W. Pacek, and M. Barigou, "Interpreting the interfacial and colloidal stability of bulk nanobubbles," Soft Matter **14**(47), 9643–9656 (2018).

[43]J. N. Meegoda, S. A. Hewage, and J. H. Batagoda, "Application of the diffused double layer theory to nanobubbles," Langmuir **35**(37), 12100–12112 (2019).

[44]H. Zhang, Z. Guo, and X. Zhang, "Surface enrichment of ions leads to the stability of bulk nanobubbles," Soft Matter **16**(23), 5470–5477 (2020).

[45]M. Li, X. Ma, J. Eisener, P. Pfeiffer, C.-D. Ohl, and C. Sun, "How bulk nanobubbles are stable over a wide range of temperatures," J. Colloid Interface Sci. **596**, 184–198 (2021).

[46]A. V. Postnikov, I. V. Uvarov, M. V. Lokhanin, and V. B. Svetovoy, "Electrically controlled cloud of bulk nanobubbles in water solutions," PLoS One **12**(7), e0181727 (2017).

[47]A. Novitsky, M. Ramanovich, and D. V. Novitsky, "Operator effective medium approximation for inhomogeneous and curvilinear media," Phys. Rev. B **108**(20), 205401 (2023).

[48]J. H. Weijs, J. R. T. Seddon, and D. Lohse, "Diffusive shielding stabilizes bulk nanobubble clusters," ChemPhysChem **13**(8), 2197–2204 (2012).